Assimilation of SeaWiFS Ocean Chlorophyll Data into a Three-Dimensional Global Ocean Model

Watson W. Gregg

NASA/Goddard Space Flight Center/Global Modeling and Assimilation Office

Code 610.1

Greenbelt, MD 20771

watson.gregg@nasa.gov

Assimilation of satellite ocean color data is a relatively new phenomenon in ocean sciences. However, with routine observations from the Sea-viewing Wide Field-of-view Sensor (SeaWiFS), launched in late 1997, and now with new data from the Moderate Resolution Imaging Spectroradiometer (MODIS) Aqua, there is increasing interest in ocean color data assimilation. Here SeaWiFS chlorophyll data were assimilated with an established three-dimensional global ocean model. The assimilation improved estimates of chlorophyll and primary production relative to a free-run (no assimilation) model. This represents the first attempt at ocean color data assimilation using NASA satellites in a global model. These results suggest the potential of assimilation of satellite ocean chlorophyll data for improving models.

Assimilation of SeaWiFS Ocean Chlorophyll Data into a Three-Dimensional Global
Ocean Model

Watson W. Gregg

NASA/Goddard Space Flight Center/Global Modeling and Assimilation Office
Code 610.1
Greenbelt, MD 20771
watson.gregg@nasa.gov

Abstract.

Sea-viewing Wide Field-of-view Sensor (SeaWiFS) chlorophyll data were assimilated with an established three-dimensional global ocean model. The assimilation improved estimates of chlorophyll relative to a free-run (no assimilation) model. Compared to SeaWiFS, annual RMS log error of the assimilation model was 7.7%. The free-run model had an RMS log error of 23.8%. In situ data were compared to the assimilation model over a 6-year time period from 1998 through 2003, generating an RMS log error of 28.4%, with a bias of 0.9% for daily coincident, co-located data. SeaWiFS RMS log error was nearly identical at 26.5% with and similarly negligible bias at 0.6%. The free-run RMS log error and bias at 43.4% and -5.4%, respectively, indicated how much the assimilation improved model results. Annual primary production estimates for the 1998-2003 period produced a nearly 50% improvement by the assimilation model over the free-run model as compared to a widely used algorithm using SeaWiFS chlorophyll data. These results suggest the potential of assimilation of satellite ocean chlorophyll data for improving models.

Introduction

Assimilation of satellite ocean color data is a relatively new phenomenon in ocean sciences. However, with routine observations from the Sea-viewing Wide Field-of-view Sensor (SeaWiFS), launched in late 1997, and now with new data from the Moderate Resolution Imaging Spectroradiometer (MODIS) Aqua, there is increasing interest in ocean color data assimilation. The main motivations for assimilation are:

1. Parameter Estimation

2. State and Flux Estimation

3. Prediction

Virtually all work in marine biological applications up to now has focused on the first two motivations. SeaWiFS has been used for parameter estimation in 0-dimensional models of the Equatorial Pacific (Freidrichs, 2002) using the adjoint method and the North Atlantic (Hemmings et al., 2003; 2004) using other variational methodologies. Garcia-Gorriz et al. (2003) developed a 3-dimensional model of the Adriatic Sea and used SeaWiFS data for both parameter and state estimation, using the adjoint method. Natvik and Evensen (2003)

took a different approach for state estimation only, using SeaWiFS chlorophyll data with an Ensemble Kalman Filter assimilation in a three-dimensional model of the North Atlantic. These initial efforts of data assimilation with modern ocean color satellite data, as well as earlier experiments with nudging (Armstrong et al. (1995) and insertion (Ishizaka, 1990) with the historical sensor, the Coastal Zone Color Scanner, have suggested the potential for using data assimilation and remote sensing to improve model parameterization and results. Studies with in situ data (e.g., Schlitzer, 2002; Spitz et al., 2001; Schartau and Oschlies, 2003; Lawson et al., 1996) as well as simulated data (e.g., Eknes and Evensen, 2002; Gunson et al., 1999) have further bolstered the case for utilizing assimilation for marine biological modeling.

Here an existing coupled general circulation, biogeochemical, and radiative model of the global oceans is used as a platform to assimilate SeaWiFS chlorophyll data products. The emphasis is on state and flux estimation; specifically, improved estimates of surface chlorophyll and depth-integrated primary production, respectively. Quantitative measures and statistical analyses are utilized to evaluate the effects of data assimilation in a global context.

Methods

Coupled Three-Dimensional Circulation/Biogeochemical/Radiative Model of the Global Ocean

A diagrammatic representation of a fully coupled general circulation/ biogeochemical/radiative model, called the NASA Ocean Biogeochemical Model (NOBM), illustrates the complex interactions among the three major components, ocean general circulation, radiative, and biogeochemical processes models (Figure 1). The Ocean General Circulation Model (OGCM) is a reduced gravity representation of circulation fields (Schopf and Loughe, 1995). It is global in scale, extending from near the South Pole to 72° N, in increments of 2/3° latitude and 1 1/4° longitude, comprising all regions where bottom depth > 200m. The model contains 14 vertical layers, in quasi-isopycnal coordinates, and is driven by wind stress, sea surface temperature, and shortwave radiation (Table 1).

The biogeochemical processes model contains 4 phytoplankton groups, 4 nutrient groups, a single herbivore group, and 3 detrital pools (Figure 2). The phytoplankton groups differ in

maximum growth rates, sinking rates, nutrient requirements, and optical properties. The 4 nutrients are nitrate, regenerated ammonium, silica to regulate diatom growth, and iron. Phytoplankton are ingested by a single herbivore component. Three detrital pools provide for storage of organic material, sinking, and eventual remineralization back to usable nutrients. This results in 12 state variables in the fully coupled model. Atmospheric deposition of iron and sea ice fields are required as an external forcing fields (Table 1). The biogeochemical processes model is described fully in the Appendix.

Radiative transfer calculations provide the underwater irradiance fields necessary to drive growth of the phytoplankton groups, and interact with the heat budget. The Ocean-Atmosphere Radiative Model (OARM, Gregg, 2002a) contains a treatment of the spectral and directional properties of radiative transfer in the oceans, and explicitly accounts for clouds. The atmospheric radiative model is based on the Gregg and Carder (1990) spectral model, extended to the spectral regions 200 nm to 4 μm. It requires external monthly climatologies of cloud properties (cloud cover and liquid water path), surface pressure, wind speeds, relative humidity, precipitable water, and ozone (Table 1). Aerosols are considered to be strictly of marine origin and are computed as in Gregg and Carder (1990).

Oceanic radiative properties are driven by water absorption and scattering, the optical properties of the phytoplankton groups, and chromophoric dissolved organic matter (CDOM). Three irradiance paths are enabled: a downwelling direct path, a downwelling diffuse (scattered) path, and an upwelling diffuse path. All oceanic radiative calculations include the spectral nature of the irradiance.

Data Assimilation

The data assimilation methodology used here is the Conditional Relaxation Analysis Method (CRAM; Oort, 1983). The method is used for bias correction in Optimal Interpolation Sea Surface Temperature (OISST) data (Reynolds, 1988; Reynolds and Smith, 1994), and has been used successfully for ocean color in situ-satellite applications (Gregg and Conkright, 2001; 2002; Conkright and Gregg, 2003). CRAM uses data insertion to provide an internal boundary condition, which here is the satellite ocean chlorophyll and solves for an analyzed chlorophyll field of model and data

$$\nabla^2 C = \nabla^2 C_M \qquad (1)$$

where C is the final analyzed field of chlorophyll and C_M is the model field (sum of the 4 phytoplankton groups). Insertion of satellite chlorophyll serves a bias-correction capability. The matching of Laplacian's of the model chlorophyll and model/satellite chlorophyll extends the bias correction away from the satellite data points, while maintaining the higher order model variability. Because of the wide range of chlorophyll over the global oceans (>3 orders of magnitude), model and satellite data were log-transformed (base 10) before application of Eq. 1. The analyzed chlorophyll was transformed back to linear form for re-initialization, and distributed among the 4 phytoplankton groups in such a way to retain the previous relative abundances.

Data assimilation was performed daily, to remove biases associated with sampling by SeaWiFS (i.e., cloud cover, sun glint, inter-orbit gaps), that are incorporated in 8-day and monthly data products. Assimilation occurred at model midnight.

The daily assimilation required daily forcing data. These were all from the same sources as in Table 1, except at daily time-varying frequencies. Daily wind stresses were weighted 80:20 percent monthly:daily to minimize transient high wind events.

CRAM is computationally very fast, so much that there is nearly negligible additional processing time in its use. However, it is very strongly weighted toward the data. Thus data errors are a very important problem in its application. For this reason, data errors must be minimized to the extent possible. In the present application, data error minimization efforts involved:

1) All daily SeaWiFS chlorophyll > 2 times the monthly mean were excluded

2) Monthly mean SeaWiFS data were weighted 25% to 75% daily data

3) SeaWiFS data occurring within a model grid point containing ice were excluded

4) Regional weighting of model and SeaWiFS chlorophyll was enforced (Figure 3)

The fourth data error minimization was based on analyses by Gregg and Casey (2004) indicating regions where SeaWiFS tended to perform poorly compared to in situ data. It was also partly based on assimilation trial-and-error: where the assimilation produced negative values of any of the model variables or where unrealistic values occurred, heavier weighting toward the model was enforced. Typically the two conditions overlapped. For example, excessively high chlorophyll concentrations were produced by the assimilation in the Congo and Amazon/Orinoco River discharges. These are regions dominated by CDOM,

which produce erroneous chlorophyll values in satellite retrievals. These regions were shown to have a poor comparison with in situ data (Gregg and Casey, 2004). Similar problems occurred with respect to regions where absorbing dust is prevalent, such as the tropical Atlantic and North and Equatorial Indian Oceans (Gregg and Casey, 2004). The regional model weighting factors used in the assimilation are shown in Figure 3. There were three variations on regional weighting that were applied seasonally. All three are shown in Figure 3.

Data Sets

Global chlorophyll data from SeaWiFS were obtained from the NASA Goddard Earth Science Distributed Active Archive Center (GES-DAAC) site at daily and monthly, 9-km resolution. The data set version number was 4.0. The data were re-mapped to the model grid before assimilation and comparison. Daily data were used for assimilation; monthly data were used for analysis.

Forcing data sets are shown in Table 1. Soil dust data sets were available only for the period Jan 2000 through Jul 2002. Climatologies were created to provide data when needed outside this period. Similarly, ISCCP cloud data were only available for Jan 1997 through Sep 2001. Again climatologies were created to fill data gap periods.

In situ chlorophyll data were obtained from the SeaWiFS Bio-Optical Archive and Storage System (SeaBASS; Werdell and Bailey, 2002) and the NOAA/National Oceanographic Data Center (NODC)/Ocean Climate Laboratory (OCL) archives (Conkright et al., 2002a). This was an updated version of the same combined data set used by Gregg and Casey (2004). The in situ data were re-mapped to the model grid on a daily basis.

Analysis

SeaWiFS chlorophyll assimilation was evaluated in the context of chlorophyll (state estimation) and primary production (flux estimation). In both cases, assimilated fields were compared to those from a free-run model (no assimilation but using the same startup distributions and forcing data). For primary production, free-run model-computed primary production was compared with model-computed primary production derived from assimilated chlorophyll and finally against primary production derived directly from satellite chlorophyll data using the Vertically Generalized Production Model (VGPM; Behrenfeld and Falkowski, 1997).

Analyses involved use of what is defined here as the Annual Root Mean Square Log Error:

$$RMS_{mon} = \sqrt{\frac{\sum [log_{10}C_{assim} - log_{10}C_{sat}]^2}{n}} \times 100 \qquad (2)$$

$$RMS_{ann} = \frac{\sum RMS_{mon}}{12} \qquad (3)$$

where RMS_{mon} is the monthly RMS log error (computed by comparing monthly mean model chlorophyll derived from assimilation (C_{assim}) with monthly mean SeaWiFS chlorophyll (C_{sat}), n is the number of co-located assimilation and SeaWiFS chlorophyll values for each month, and RMS_{ann} is the annual RMS log error, which is simply the mean of the monthly RMS log errors over 12 months of a year. This methodology keeps the sense of the monthly deviations of the assimilation from SeaWiFS, unlike comparing data from an annual mean, while producing a single value over an entire year.

Assimilation model annual RMS log errors were evaluated by comparison with those from the free-run (control) model. The assimilation frequency was also adjusted, by assimilating every 2 days, 3 days, etc. instead of daily assimilation, to observe error growth.

Additionally, SeaWiFS, free-run model, and assimilation model chlorophyll were compared against the large data base of in situ chlorophyll data from NASA/SeaBASS and NOAA/NODC. Analyses involved use of the RMS log error defined similarly to the monthly analysis define in Eq. 2 except compiling all daily data over the 6-year time span into a single representation of RMS log error, where in situ data and satellite/model data were coincident and co-located. Bias is defined as the mean error the daily coincident, co-located in situ and satellite/model data

$$Bias = \frac{\sum [\log_{10}C_{assim} - \log_{10}C_{sat}]}{n} \times 100 \qquad (4)$$

Primary production provided a means to evaluate the ability of the assimilation model to improve flux estimates. Primary production was computed in the model as a function of growth rate multiplied by the carbon:chlorophyll ratio:

$$PP = \int \sum \mu_i C_i \, \Phi \, dz \qquad (5)$$

where μ_i is the realized new growth rate of phytoplankton component i, C_i is the chlorophyll concentration of component i, Φ is the carbon:chlorophyll ratio, and the product is integrated over depth. Assimilation of chlorophyll affected the total chlorophyll but not the relative abundances of the phytoplankton groups, μ, or Φ directly. All three can be affected by the assimilation of chlorophyll indirectly, however, by changing the irradiance in the water column and the horizontal and vertical gradients of phytoplankton and nutrients. Primary production computed by the free-run model and the assimilation model were intercompared, and also were evaluated against an independent estimate by the VGPM. The VGPM requires chlorophyll, SST, and photosynthetically available radiation (PAR) as inputs. Chlorophyll was taken from SeaWiFS, SST was the same source as used for model forcing (Table 1), and PAR was derived from the atmospheric component of OARM, with wavelength region 350-700 nm selected and converted to quanta.

Results and Discussion

NOBM

Minor changes in NOBM (see Appendix) necessitated evaluation to ensure its performance did not degrade from Gregg et al. (2003). In the 50th year of model execution using climatological monthly forcing, basin-scale seasonal chlorophyll variability from the model was statistically positively correlated ($P < 0.05$) with those determined from SeaWiFS monthly climatological chlorophyll in each of the 12 major oceanographic basins of the world, (see Figure 3) except the Equatorial Pacific, which exhibited very little

seasonal variability. Global annual chlorophyll was 18.2% lower than SeaWiFS, with an annual RMS log error of 25.4%. Annual mean log-transformed dissolved iron concentrations in the model surface layer were positively correlated with observations ($P <$ 0.05) over the 10 (out of 12) major oceanographic basins where data were available (1951 in situ data records derived from the general literature). The basins where dissolved iron data were lacking were the South Indian and South Atlantic (see Figure 3).

Overall patterns of phytoplankton functional group distributions exhibited broad qualitative agreement with in situ data (359 surface layer observations). Three of the four phytoplankton groups exhibited statistically significant correspondence across basins. Chlorophytes did not. Chlorophytes are a transitional group in the model, and they represent a wide range of phytoplankton, such as flagellates, Phaeocystis spp., etc. This expectation is probably unrealistic, which accounts for the lack of statistical significance in their relative abundances. However, it is encouraging that diatoms, cyanobacteria, and coccolithophore annual mean relative abundances were statistically positively correlated with data.

SeaWiFS Assimilation 2001

Model execution for 2001 using daily forcing was used to evaluate the effectiveness of chlorophyll assimilation. Basin-scale seasonal variability for both the free-run and assimilation models were statistically positively correlated with SeaWiFS in all 12 major basins, but the correlation coefficients for the assimilation model were much higher (Table 2). This suggests the lack of significance for the Equatorial Pacific in the climatological model was due to use of climatological forcing.

Daily assimilated satellite chlorophyll from SeaWiFS for April 1 compared favorably with monthly mean SeaWiFS data (Figure 4). Although there was broad agreement between the free-run model and SeaWiFS monthly, the improvement using assimilation was clear. SeaWiFS chlorophyll for the same day as the free run and assimilated models is also shown, but because of cloud obscuration, sun glint, a sensor tilt change, and inter-orbit gaps, it is difficult to evaluate the comparison. This illustrates the additional usefulness of assimilation, in providing complete daily coverage.

A more quantitative description of the effectiveness of assimilation is provided using monthly means of the assimilation model and SeaWiFS, and taking the difference (Figure 5). For March 2001, the overall similarity of the assimilation and SeaWiFS was evident,

and largely supported by the difference field. The largest differences occurred in the Arabian Sea, the Congo mouth, and the Mauritanian coast. All of these are by design in the assimilation model, with model weighting factors largest in these areas of low confidence in SeaWiFS. In all cases the differences were underestimates by the assimilation model, which is desired. Other smaller differences occurred in the northern extremities of the North Atlantic, the Pacific in the extreme western edge of the Bering Sea, and in the Atlantic sector of the Southern Ocean. Again the differences were underestimates by the assimilation. Overestimates by the assimilation were generally small (0.01-0.05 mg m^{-3} chl). A couple of notable exceptions were offshore of the Somalian coast, and the east-central Indian Ocean, where overestimates by the model of 0.05-0.1 mg m^{-3} occur.

Similar results occurred for Sep 2001 (Figure 6). Again the overall agreement between the assimilation model and SeaWiFS was good, with disparities in similar regions, specifically the Congo and Orinoco River outflows, the Arabian Sea, and the upper northern latitudes. There was a band in the Equatorial Atlantic where the assimilation model overestimated SeaWiFS, that did not appear related to the Congo River.

The growth of error as a function of assimilation frequency was tracked using the annual RMS log error (Figure 7). Using daily assimilation, the annual RMS log error was 7.7% relative to SeaWiFS, which was a very large improvement over the error for the free-run model at 23.8%. The error grew as the assimilation frequency decreased. It was still <10% if the assimilation occurred every 3 days. It stayed below 15% for assimilations occurring every 10 days or less. At the other extreme, very low assimilation frequencies, the annual RMS log error approached the free-run model. The lowest assimilation frequency was once per year (every 183 days) for which the error is indistinguishable from the free-run model.

SeaWiFS Assimilation 1997-2003

A long-term run of the free-run model and the assimilation model for 1997-2003 using monthly forcing illustrates the improvement of assimilation in the major oceanographic basins (Figure 8). The free-run model produced seasonal variability in good agreement with SeaWiFS basin mean chlorophyll, and also good correspondence with low biases in many of the basins, such as the North Central Pacific, North Atlantic, Equatorial Pacific, South Indian, South Atlantic (Figure 8a). There were several basins where a substantial bias was apparent in the free-run model. This was particularly true in the North Indian and Equatorial

Atlantic, where a large underestimate by the model occurred, but also in the spring bloom peaks in the North Pacific and Antarctic basins, with underestimates and overestimates buy the model, respectively.

The assimilation model kept the seasonal variability agreement with SeaWiFS that the free-run model demonstrated, but additionally reduced the basin mean biases (Figure 8b). The Antarctic and North Central Atlantic, which in the free-run model exhibited substantial biases, were now in nearly complete agreement. The large departure in the North Central Atlantic in autumn 1998 corresponded to a massive dust plume arising from northwestern Africa that was apparently undetected by the SeaWiFS processing algorithms (Gregg, 2002b). It was excluded by the assimilation here. The North Indian and Equatorial Atlantic showed improvement in the assimilation model, but still underestimated SeaWiFS. Model weighting factors were very high in these basins because of low confidence in SeaWiFS data (Gregg and Casey, 2004).

The assimilation model continued to underestimate the North Atlantic and North Pacific spring bloom maximum (Figure 8b). In the North Atlantic, the underestimation appeared to be worse in the assimilation than in the free-run model. However, the distribution of chlorophyll over the North Atlantic was improved by the assimilation, as noted earlier (Figure 4). The very high spring bloom peaks in SeaWiFS in the North Pacific were not simulated well by either the free-run or assimilation models. Most of the high values were derived from extremely high SeaWiFS chlorophyll in the western Bering Sea, near Kamchatka.

A detailed comparison of the models with in situ data again showed major improvement by assimilation. RMS log error of the SeaBASS/NODC in situ chlorophyll archive against SeaWiFS was 26.5%, with a nearly negligible bias of 0.6% (Table 3). The free-run model performed much more poorly against the in situ data set than SeaWiFS: 43.4% RMS log error and -5.4% bias. The assimilation model was only slightly worse than SeaWiFS compared to the in situ data set, with a 28.4% RMS log error and 0.9% bias. More importantly, the assimilation model (as well as the free-run model) had more than twice the number of coincident, co-located in situ/model matchup data points. This is a consequence of the absence of gaps in the model record in contrast to SeaWiFS.

Global annual primary production estimates from three sources, the VGPM, free-run model, and assimilation model, indicated reasonably good correspondence over the 6-year time series for which SeaWiFS data were used in this effort (Figure 9). Interannual variability was mimicked among all three estimates, with a slight departure in 2003, when the free run model indicated a slight increase from 2002, while the VGPM indicated a slight decrease. The assimilation model indicated very little change. The mean of the 6-year time series indicated that the free-run model overestimated PP as derived from VGPM by nearly 14%. The assimilation model reduced the overestimate by nearly half, producing a more minor overestimate of 7.2%.

Summary

Assimilation of chlorophyll data from SeaWiFS exhibited substantial improvements over free-run simulations. Biases in basin means were reduced, and annual RMS log errors compared to SeaWiFS were much lower for the assimilation model (7.7%) than the free-run model (23.8%). This represented a 3-fold improvement. When compared to in situ data for the 6-year time period from 1998 through 2003, the assimilation model had an RMS log error of 28.4%, with a bias of 0.9% for daily coincident, co-located data. SeaWiFS RMS log error was slightly lower at 26.5% with and similarly negligible bias at 0.6%. The free-run RMS log error and bias at 43.4% and -5.4%, respectively, indicated how much the assimilation improved model results. Annual primary production indicated a smaller improvement (mean difference from VGPM=7.2% for the assimilation model versus 13.8% for the free-run model), representing an improvement of nearly a factor of 2, assuming the validity of the VGPM. These results suggest promise for assimilation of satellite ocean chlorophyll into global models. But they also point to areas of needed improvement. The fact that the assimilated variable shows the most improvement is not surprising, and is an important attribute for data assimilation. The fact that flux (primary production) exhibited less improvement than biomass (chlorophyll) using assimilation suggests the model continues to trend in the wrong direction despite assimilation. It also suggests that similar results may be expected for other non-assimilated variables, such as phytoplankton group distributions and nutrients. There remains considerable work to be done on assimilation of satellite ocean color, such as better handling of ocean color data errors, utilizing other model

variables in a multi-variate solution, accounting for subsurface changes, as well as investigating the potential for using other ocean color products, such as diffuse attenuation coefficient at 490 nm, and potentially new products such as particulate organic carbon and calcite. Nevertheless, there is much potential in ocean color assimilation, and this effort is intended to represent an initial attempt on a global scale.

Acknowledgements

References

Agawin, N.S.R., C.M. Duarte, and S. Agusti, 2000. Nutrient and temperature control of the contribution of picoplankton to phytoplankton biomass and production. Limnology and Oceanography 45, 591-600.

Agawin, N.S.R., C.M. Duarte, and S. Agusti, 1998. Growth and abundance of *Synechococcus* sp. in a Mediterranean Bay: Seasonality and relationship with temperature. Marine Ecology Progress Series 170, 45-53.

Anning, T., H.L. MacIntyre, S.M. Pratt, P.J. Sammes, S. Gibb, and R.J. Geider, 2000. Photoacclimation in the marine diatom *Skeletonema costatum*. Limnology and Oceanography, 45, 1807-1817.

Armstrong, R.A., Sarmiento, J.L., Slater, R.D., 1995. Monitoring ocean productivity by assimilating satellite chlorophyll into ecosystem models. In: Powell, Steele (Eds.), Ecological Time Series, Chapman and Hall, London, pp. 371-390.

Behrenfeld, M.J. and P.G. Falkowski, 1997. Photosynthetic rates derived from satellite-based chlorophyll concentrations. Limnol. Oceanogr., 42: 1-20.

Carpenter, E.J. and K. Romans, 1991. Major role of the cyanobacterium *Trichodesmium* in nutrient cycling in the North Atlantic Ocean. Science, 254, 1356-1358.

Conkright, M.E. and W.W. Gregg, 2003. Comparison of chlorophyll climatologies: in situ, CZCS, blended in situ-CZCS, and SeaWiFS. International Journal of Remote Sensing, 24: 969-991.

Conkright, M.E., Antonov, J.I., Baranova, O., Boyer, T.P., Garcia, H.E., Gelfeld, R., Johnson, D., O'Brien, T.D., Smolyar, I., & Stephens, C., 2002a. World ocean database 2001, Vol. 1: Introduction. S. Levitus, Ed., NOAA Atlas NESDIS 42, US Govt. Printing Office, Washington, DC, 167 pp.

Conkright, M. E., H. E. Garcia, T. D. O'Brien, R. A. Locarnini, T. P. Boyer, C. Stephens J. I. Antonov, 2002b. World Ocean Atlas 2001, Volume 4: Nutrients. S. Levitus, Ed.,

NOAA Atlas NESDIS 52, U.S. Government Printing Office, Wash., D.C., 392 pp., CD-ROMs.

Csanady, G.T., Mass transfer to and from small particles in the sea, Limnol. Oceangr., 31,237-248, 1986.

Eppley, R.W., 1972. Temperature and phytoplankton growth in the sea. Fisheries Bulletin 70, 1063-1085.

Eknes, M., Evensen, G., 2002. An ensemble Kalman filter with a 1-D marine ecosystem model. J. Mar. Sys. 36: 75-100.

Freidrichs, M.A.M., 2002. Assimilation of JGOFS EqPac and SeaWiFS data into a marine ecosystem model of the central equatorial Pacific Ocean. Deep-Sea Res. II 49: 289-320.

Fritz, J.J. and W.M. Balch, 1996. A light-limited continuous culture study of *Emiliana huxleyi*: Determination of coccolith detachment and its relevance to cell sinking. Journal of Experimental Marine Biology and Ecology 207, 127-147.

Fung, I.Y., Meyn, S.K., Tegen, I., Doney, S.C., John, J.G., Bishop, J.K.B., 2000. Iron supply and demand in the upper ocean. Global Biogeochemical Cycles, 14, 281-295.

Garcia-Gorriz, E., Hoepffner, N., Ouberdous, M., 2003. Assimilation of SeaWiFS data in a coupled physical-biological model of the Adriatic Sea. J. Mar. Sys. 40-41: 233-252.

Ginoux, P., M. Chin, I. Tegen, J.M. Prospero, B. Holben, O. Dubovik, and S.-J. Lin, 2001. Sources and distributions of dust aerosols simulated with the GOCART model. J. Geophys. Res. 106, 20255-20273.

Gregg, W.W. and N.W. Casey, 2004. Global and regional evaluation of the SeaWiFS chlorophyll data set. Remote Sensing of Environment 93: 463-479.

Gregg, W.W. and M.E. Conkright, 2002. Decadal changes in global ocean chlorophyll. Geophysical Research Letters 29 (11): 10.1029/2002GL014689.

Gregg, W.W., 2002a. A coupled ocean-atmosphere radiative model for global ocean biogeochemical models. NASA Global Modeling and Assimilation Series, M. Suarez, ed. NASA Technical Memorandum 2002-104606, Vol. 22, 33 pp. (available using anonymous ftp at salmo.gsfc.nasa.gov, pub/outgoing/reprints/gregg_NASATM2002.pdf)

Gregg, W.W., 2002b. Tracking the SeaWiFS record with a coupled physical/biogeochemical/radiative model of the global oceans. Deep-Sea Research II 49: 81-105.

Gregg, W.W. and M.E. Conkright, 2001. Global seasonal climatologies of ocean chlorophyll: Blending in situ and satellite data for the Coastal Zone Color Scanner era. Journal of Geophysical Research, 106: 2499-2515.

Gregg, W.W. and J.J. Walsh, 1992. Simulation of the 1979 spring bloom in the Mid-Atlantic Bight: A coupled physical/ biological/optical model, J. Geophys. Res., 97, 5723-5743.

Gregg, W.W. and K.L. Carder, 1990. A simple spectral solar irradiance model for cloudless maritime atmospheres. Limnol. Oceanogr. 35: 1657-1675.

Gunson, J., Oschlies, A., Garcon, V., 1999. Sesnitivity of ecosystem parameters to simulated satellite ocean color data using a coupled physical-biological model of the North Atlantic. J. Mar. Res. 57: 613-639.

Hemmings, J.C.P., Srokosz, M.A., Challenor, P., Fasham, M.J.R., 2003. SAssimilating satellite ocean-colour observations into oceanic ecosystem models. Phil Trans. Royal Soc. London A-Math. Phys., and Eng. Sci. 361:33-39.

Hemmings, J.C.P., Srokosz, M.A., Challenor, P., Fasham, M.J.R., 2004. Split-domain calibration of an ecosystem model using satellite ocean colour data. J. Mar. Sys. 50: 141-

179.

Ishizaka, J., 1990. Coupling of Coastal Zone Color Scanner data to a physical-biological model of the southeastern United-States continental-shelf ecosystem .3. Nutrient and phytoplankton fluxes and CZCS data assimilation. J. Geophys. Res. 95: 20201-20212.

Lawson, L.M., Hofmann, E.E., Spitz, Y.H., 1996. Time series sampling and data assimilation in a simple marine ecosystem model. Deep-Sea Res. II 43: 625-651.

McGillicuddy, D.J., J.J. McCarthy, and A.R. Robinson, 1995. Coupled physical and biological modeling of the spring bloom in the North Atlantic (I): Model formulation and one dimensional bloom processes, Deep-Sea Res., 42, 1313-1357.

Moore, J.K., Doney, S.C. and Lindsay, K., 2004. Upper ocean ecosystem dynamics and iron cycling in a global three-dimensional model. Global Biogeochemical Cycles 18, doi: 10.1029/2004GB002220.

Natvik, L.J., and G. Evensen, 2001. Assimilation of ocean colour data into a biochemical model of the North Atlantic. Part 1. Data assimilation experiments. J. Mar Sys. 40-41:127-153.

Oort, A.H., 1983. Global atmospheric circulation statistics, 1958-1973, NOAA Professional Paper 14, 180 pp.

Reynolds, R.W. and T.M. Smith, 1994. Improved global sea surface temperature analyses using optimum interpolation. J. Clim. 7: 75-86.

Reynolds, R.W., 1988. A real-time global sea surface temperature analysis. J. Clim. 1: 75-86.

Schartau, M., A. Oschlies, A., 2003. Simultaneous data-based optimization of a 1D-ecosystem model at three locations in the North Atlantic: Part I – Method and parameter estimates. J. Mar. Res. 61: 765-793.

Schlitzer, R., 2002. Carbon export fluxes in the Southern Ocean: Results from inverse modeling and comparison with satellite-based estimates. Deep-Sea Res. II 49: 1623-1644.

Schopf, P.S. and A. Loughe, 1995. A reduced gravity isopycnal ocean model: Hindcasts of El Nino. Mon. Wea. Rev. 123: 2839-2863.

Spitz, Y.H., Moisan, J.R., Abbott, M.R., 2001. Configuring an ecosystem model using data from the Bermuda Atlantic Time Series (BATS). Deep-Sea Res. II 48: 1733-1768.

Werdell, P.J. and S.W. Bailey, 2002. The SeaWiFS Bio-Optical Archive and Storage System (SeaBASS): Current Architecture and Implementation. *NASA Technical Memorandum 2002-211617*, G.S. Fargion and C.R. McClain, eds. NASA Goddard Space Flight Center, Greenbelt, MD.

Table 1. Forcing data sets required to force NOBM, their purpose, and sources of data. NCEP is the National Center for Environmental Prediction, TOMS is the Total Ozone Mapping Spectrometer, ISCCP is the International Satellite Cloud Climatology Project, OISST is the Optimum Interpolated Sea Surface Temperature product, and GOCART is the Global Ozone Chemistry Aerosol Radiation and Transport model (Ginoux et al., 2001). Daily data are used for the 2001 assimilation analyses, and monthly data are used for the 1997-2003 analyses.

General Circulation Model

Variable	*Purpose*	*Source*
Wind stress	Surface forcing	NCEP Reanalysis
Sea surface temperature	Surface forcing	OISST
Shortwave radiation	Surface forcing	NCEP Reanalysis

Biogeochemical Process Model

Variable	*Purpose*	*Source*
Aerosol composition	Surface input (iron)	GOCART
Sea ice	Surface forcing	OISST

Radiative Transfer Model

Variable	*Purpose*	*Source*
Wind speed	Surface reflectance/Aerosols	NCEP Reanalysis
Precipitable water	Water vapor absorption	NCEP Reanalysis
Surface pressure	O_2 absorption/Rayleigh scattering	NCEP Reanalysis
Relative humidity	Marine aerosols	NCEP Reanalysis
Ozone	Gaseous absorption	TOMS
Cloud cover	Cloud distribution	ISCCP
Cloud liquid water path	Cloud attenuation properties	ISCCP

Table 2. Mean annual basin difference from SeaWiFS for the free-run and the assimilation model, and the correlation coefficients (r) for the correlation with SeaWiFS seasonal variability for 2001. An asterisk indicates the correlation is significant at P<0.05

Basin	Free-run Model Difference	r	Assimilation Model Difference	r
North Atlantic	-40.4%	0.888*	-22.8%	0.993*
North Pacific	-43.9%	0.623*	-29.8%	0.860*
North Central Atlantic	-37.1%	0.854*	-20.4%	0.810*
North Central Pacific	27.6%	0.962*	1.5%	0.995*
North Indian	-67.9%	0.765*	-53.5%	0.822*
Equatorial Atlantic	-48.2%	0.687*	-29.1%	0.909*
Equatorial Pacific	-10.8%	0.718*	-5.3%	0.975*
Equatorial Indian	-27.4%	0.934*	-16.0%	0.977*
South Atlantic	9.8%	0.775*	-10.0%	0.979*
South Pacific	60.3%	0.660*	2.4%	0.988*
South Indian	42.6%	0.624*	5.5%	0.998*
Antarctic	6.6%	0.909*	-9.7%	0.976*

Table 3. Statistics for the comparison of SeaBASS/NODC chlorophyll data for the period 1998-2003 with coincident, co-located SeaWiFS, free-run model and assimilation model chlorophyll. N indicates the number of points where in situ and satellite/model points were coincident and co-located.

	RMS log Error	log Bias	N
SeaWiFS	26.5%	0.6%	2133
Free-run Model	43.4%	-5.4%	4471
Assimilation Model	28.4%	0.9%	4471

Appendix. Biogeochemical processes model description.

NOBM is based on Gregg et al. (2003). There are several new features in the biogeochemical processes model component:

-- new maximum phytoplankton growth rates at 20°C

-- full detrital dynamics with 3 components, fully coupled to the OGCM

-- a new formulation for the temperature-dependence for grazing

-- a new formulation for nitrogen fixation for the cyanobacteria component

-- introduction of dissolved iron scavenging and an increase in atmospheric iron solubility

-- new nitrogen half-saturation constants for chlorophytes

-- new iron half-saturation constants for chlorophytes and cyanobacteria

Other aspects of the biogeochemical processes model are described in Gregg et al (2003), but are provided here for completeness.

The governing equations of the model are

Phytoplankton

$$\frac{\partial}{\partial t} C_i = \nabla(K\nabla C_i) - \nabla\bullet VC_i - \nabla\bullet(w_s)_i\, C_i + \mu_i C_i - gH - sC_i \tag{A1}$$

$i = 1 = $ diatoms
$i = 2 = $ chlorophytes
$i = 3 = $ cyanobacteria
$i = 4 = $ coccolithophores

Nutrients

$$\frac{\partial}{\partial t} N_N = \nabla(K\nabla N_N) - \nabla\bullet VN_N - b_n[\Sigma_i\, \mu_i C_i] + r_n D_C/(C{:}N) \tag{A2}$$

$$\frac{\partial}{\partial t} N_A = \nabla(K\nabla N_A) - \nabla\bullet VN_A - b_n[\Sigma_i\, \mu_i C_i] + b_n\varepsilon[gH + n_2 H^2] \tag{A3}$$

$$\frac{\partial}{\partial t} N_S = \nabla(K\nabla N_S) - \nabla\bullet VN_S - b_s\mu_1 C_1 + r_s D_s \tag{A4}$$

$$\frac{\partial}{\partial t} N_I = \nabla(K\nabla N_I) - \nabla\bullet VN_I - b_f[\Sigma_i\, \mu_i C_i] + b_f\varepsilon[gH + n_2 H^2] + r_f D_I + A/L - M \tag{A5}$$

∂t

N_N = nitrate
N_A = ammonium
N_S = silica
N_I = dissolved iron

Herbivores
$$\frac{\partial}{\partial t} H = \nabla(K\nabla H) - \nabla \bullet \mathbf{V}H + (1-\varepsilon)gH - n_1 H - n_2 H^2 \tag{A6}$$

Detritus
$$\frac{\partial}{\partial t} D_C = \nabla(K\nabla D_C) - \nabla \bullet (\mathbf{w_d})_C D_C - r_c D_C + \Phi[s\Sigma_i\, C_i + n_1 H] + \Phi(1-\varepsilon)\, n_2 H^2 \tag{A7}$$

$$\frac{\partial}{\partial t} D_S = \nabla(K\nabla D_S) - \nabla \bullet (\mathbf{w_d})_S D_S - r_s D_S + b_s[sC_1 + gH] \tag{A8}$$

$$\frac{\partial}{\partial t} D_I = \nabla(K\nabla D_I) - \nabla \bullet (\mathbf{w_d})_I D_I - r_f D_I + b_f[s\Sigma_i\, C_i + n_1 H] + b_f(1-\varepsilon)\, n_2 H^2 + M \tag{A9}$$

D_N = carbon/nitrogen detritus
D_S = silica detritus
D_I = iron detritus

where the symbols and values are identified in Appendix Table 1. Bold denotes a vector quantity. All biological processes are assumed to cease in the presence of sea ice, which is included as an external forcing field.

Phytoplankton

The growth formulation includes dependence on total irradiance (E_T), nitrogen as nitrate plus ammonium (N_T), silica (Si – for diatoms only), iron (Fe), and temperature (T)

$$\mu_i = \mu_{mi}\, \min[\mu(E_T)_i, \mu(N_T)_i, \mu(Si)_i,\, \mu(Fe)_i]\, \mu(T)\beta_i \tag{A10}$$

where i indicates the phytoplankton functional group index (in order, diatoms, chlorophytes, cyanobacteria, and coccolithophores), μ is the total specific growth rate (d^{-1}) of phytoplankton,

μ_m is the maximum growth rate at 20°C (Appendix Table 1). The term $\mu(E_T)$ represents the growth rate as a function solely of the total irradiance (μmol quanta m^{-2} s^{-1}),

$$\mu(E_T) = \frac{E_T}{(E_T + k_E)} \tag{A11}$$

where k_E is the irradiance at which $\mu = 0.5\mu_m$ and equals 0.5 I_k, where I_k is the light saturation parameter. The nutrient-dependent growth terms are

$$\mu(NO_3)_i = \frac{NO_3}{[NO_3 + (k_N)_i]} \tag{A12}$$

$$\mu(NH_4)_i = \frac{NH_4}{[NH_4 + (k_N)_i]} \tag{A13}$$

$$\mu(N_T)_i = \mu(NH_4)_i + \min[\mu(NO_3)_i, 1-\mu(NH_4)_i] \tag{A14}$$

(Gregg and Walsh, 1992)

$$\mu(Si)_i = \frac{Si}{[Si + (k_S)_i]} \tag{A15}$$

$$\mu(Fe)_i = \frac{Fe}{[Fe + (k_F)_i]} \tag{A16}$$

Temperature-dependent growth is from Eppley (1972)

$$\mu(T) = 1.066^{(T-20)} \tag{A17}$$

which produces a temperature-growth factor normalized to 20°C. The term β in Eq. A10 is an additional adjustment used for the cyanobacteria component that reduces their growth rate in cold water (<15°C)

$$\beta_3 = 0.0294T + 0.558 \tag{A18}$$

$\beta_i = 1$ for the other three phytoplankton components (i=1,2,4). This effect conforms to observations that cyanobacteria are scarce in cold waters (Agawin et al., 2000; 1998). The cyanobacteria component possesses a modest ability to fix nitrogen from the water column, as

observed in *Trichodesmium* spp. (Carpenter & Romans 1991). The nitrogen fixation is expressed as additional growth occurring when nitrogen availability is $<(k_N)_3$,

$$\mu_{nfix} = 0.25\exp(-75C_3) \tag{A19}$$

where the index 3 indicates cyanobacteria. The biomass dependence represents a progressive community changeover from non-N-fixing cyanobacteria to N-fixing bacteria as the total population declines under nitrogen-stressed conditions. The total N-limited growth rate plus the additional growth derived from N-fixation is not allowed to exceed the growth rate where total nitrogen $= (k_N)_3$. No accounting for denitrification is made in the model.

Photoadaptation is simulated by stipulating 3 states: 50, 150 and 200 (μmol quanta m^{-2} s^{-1}). This is based on laboratory studies which typically divided experiments into low, medium, and high classes of light adaptation. Carbon:chlorophyll ratios (Φ) correspond to the photoadaptation state, to represent the tendency of phytoplankton to preferentially synthesize chlorophyll in low light conditions, to enable more efficient photon capture. The three Φ states corresponding to the three light states are 25, 50 and 80 g g^{-1}. The Φ results for diatoms in the model closely mimick Anning et al.'s (2000) results for diatoms. For irradiance levels falling between the three light states, the C:chl ratios are linearly interpolated.

Mean irradiance is computed during daylight hours, and then the phytoplankton photoadaptive state is classified accordingly. This calculation is only performed once per day to simulate a delayed photoadaptation response. Light saturation constants for the three light levels are provided in Appendix Table 1.

Phytoplankton vector sinking is treated as additional advection in the z-direction, and is given at 31°C, representing approximately the maximum. It is adjusted by viscosity according to Stokes Law (Csanady, 1986), which is parameterized here by temperature

$$w_s(T) = w_s(31)[0.451 + 0.0178T] \tag{A20}$$

Coccolithophore sinking rates were allowed to vary as a function of growth rate from 0.3 to 1.4 m d^{-1} based on observations by Fritz and Balch (1996). A linear relationship was assumed

$$w_{s4} = 0.752\mu_{m4} + 0.225 \tag{A21}$$

where w_s is the sinking rate of coccolithophores (m d^{-1}), μ_m is the maximum growth rate actually achieved, and the subscript 4 represents coccolithophores..

Nutrients

The diversity in the processes affecting the four nutrient groups requires elucidation in 4 separate equations, unlike the phytoplankton. All are taken up by phytoplankton growth, with silica subject only to diatom uptake (note the subscript=1 in Eq. A4 denoting diatoms). For three of the nutrients, nitrate, silica, and dissolved iron, corresponding detrital pools remineralize to return nutrients previously uptaken by phytoplankton. There is no detrital pool for ammonium, which is excreted as a function of herbivore grazing, and as a function of higher order ingestion of herbivores, represented by the term n_2H^2 in Eqs. A3, A5, A6, A7, and A9. Dissolved iron also has an excretion pathway, but nitrate and silica do not. The nutrient to chlorophyll ratios, denoted b in Eqs. A2-A5, are derived from Redfield ratios, which are constant (Appendix Table 1) and the carbon:chlorophyll (Φ) ratio which is not.

$$b_n = \Phi/C:N \qquad\qquad (A22)$$

$$b_s = \Phi/C:S \qquad\qquad (A23)$$

$$b_i = \Phi/C:Fe \qquad\qquad (A24)$$

This leads to variable nutrient to chlorophyll ratios in the model.

As in Gregg et al. (2003) dust deposition fields are derived from Ginoux et al. (2001). In this model, four dust size fractions are transported, corresponding to clay (smallest) and three increasing fractions of silt. The iron content is assumed to vary among the clay and silt fractions as follows: clay = 3.5% iron, silt = 1.2% iron (Fung et al., 2000). Iron solubility is assumed at 2% for all fractions, which is toward the low end of current estimates (Fung et al., 2000), but is the same as used by Moore et al. (2004).

Herbivores

Grazing uses an Ivlev formulation (McGillicuddy et al., 1995),

$$g(T) = R(T)[1-\exp(-\Lambda\Sigma_iC_i)] \qquad\qquad (A25)$$

$R(T)$ is the maximum grazing rate at $20°$ C (R_m) adjusted by temperature

$$R(T) = R_m[0.06\exp(0.1T) + 0.70] \qquad\qquad (A26)$$

The temperature-dependence for grazing is more linear than that for phytoplankton, reflecting the larger size of their overall community. The grazing represents the total loss of phytoplankton to herbivores, as indicated by the summation symbol, but is applied to the individual

phytoplankton functional groups proportionately to their relative abundances. This enables herbivore grazing to adapt the prevailing phytoplankton community.

The two loss terms in Eq. A6 represent the death of herbivores (n_1H) and higher order heterotrophic losses (n_2H^2). These formulations and parameters (Appendix Table 1) were taken from McGillicuddy et al. (1995).

Detritus

Three detrital components represent the three major nutrient elements, carbon/nitrogen, silica, and iron. The nitrogen detritus is kept as carbon in the model, but since the C:N ratio is constant, it is simple to convert when needed. All are subject to advection, diffusion and sinking. Detrital sinking, like phytoplankton sinking, is dependent on viscosity parameterized here in terms of temperature, using the same formulation. Remineralization is also temperature-dependent, but uses the phytoplankton growth-dependence term Eq. A17. Silica contained in the diatom component of phytoplankton is assumed to pass through herbivores upon grazing directly into the silica detritus pool. No silica remains in the herbivore component at any time.

Initial Conditions

NOBM underwent a spin-up of a total of 50 years under climatological forcing. For the first 20 years, initial dissolved iron conditions were from Fung et al. (2000), and nitrate and silica distributions were from annual climatologies from National Oceanographic Data Center (NODC; Conkright et al., 2002b). Ammonium initial conditions were set to $0.5\mu M$. Initial conditions for all phytoplankton groups and herbivores were set to 0.05 mg m^{-3} chl throughout the entire model domain. Initial conditions for detritus were set to 0. After 20 years, dissolved iron and detritus distributions were retained, while all other fields were reset to their original values. The model was run again for 30 years. This methodology enables dissolved iron to reach steady state without adversely impacting phytoplankton group distributions with excessively low initial values.

Appendix Table 1. Notation and parameters and variables for NOBM. Values are provided for the parameters and ranges are provided for the variables. When a parameter varies according to temperature, the value at a specified temperature is shown and identified. Nutrient/chlorophyll ratios are variable because of photadaptation-dependence, and only the range is shown, corresponding to low-, and high-light adaptation, and therefore also corresponding to C:chl ratios of 20 and 80 g g^{-1}.

Symbol	Parameter/Variable	Value	Units
General			
K	Diffusivity	Variable	m^2 s^{-1}
∇	Gradient operator	none	none
V	Vector velocity	Variable	m s^{-1}
L	Layer thickness	Variable	m
Phytoplankton			
w$_s$	Vector sinking rate of phytoplankton at 31°C		m d^{-1}
	diatoms	1.0	
	chlorophytes	0.25	
	cyanobacteria	0.0085	
	coccolithophores	0.3-1.4	
μ	Specific growth rate of phytopl. At 20°C		d^{-1}
	diatoms	1.50	
	chlorophytes	1.26	
	cyanobacteria	1.00	
	coccolithophores	1.13	
I$_k$	Light Saturation		μmol quanta m^{-2} s^{-1}

	Light level:	Low (50)	Medium (150)	High (200)
	diatoms	90.0	93.0	184.0
	chlorophytes	96.9	87.0	143.7
	cyanobacteria	65.1	66.0	47.0
	coccolithophores	56.1	71.2	165.4

Symbol	Parameter/Variable	Value	Units
s	Senescence	0.05	d^{-1}
Nutrients (N)			
C:N	Carbon:nitrogen ratio	79.5	μg l^{-1} (μM)$^{-1}$
C:S	Carbon:silica ratio	79.5	μg l^{-1} (μM)$^{-1}$
C:Fe	Carbon:iron ratio	1800	μg l-1 (nM)$^{-1}$
b	Nutrient:chlorophyll ratio		μM (μg l^{-1})$^{-1}$
	nitrogen	0.3 – 1.0	
	silica	0.3 – 1.0	
	iron	0.01 – 0.04	
ε	Nutrient excretion		d^{-1}
	nitrate	0.0	
	ammonium	0.25	
	silica	0.0	

		iron	0.25	
A	Atmospheric deposition of iron		0.03-967.0	nmol m^{-2} d^{-1}
$k_{N,S,F}$	Half-saturation constant			
	nitrogen			μM
		diatoms	1.0	
		chlorophytes	0.67	
		cyanobacteria	0.50	
		coccolithophores	0.50	
	silica			μM
		diatoms	0.2	
	iron			nM
		diatoms	1.0	
		chlorophytes	0.78	
		cyanobacteria	0.67	
		coccolithophores	0.67	
M	Iron scavenging rate			d^{-1}
	Low iron (<0.06nM)		2.0×10^{-4}	
	High iron ($\geq$0.06nM)		2.0×10^{-3}	

Herbivores (H)

R_m	Maximum grazing rate at 20° C		1.0	d^{-1}
Λ	Ivlev constant		1.0	(μg l^{-1})$^{-1}$
n_1, n_2	Heterotrophic loss rates		0.1,0.5	d^{-1}

Detritus (D)

w_d	Vector sinking rate of detritus at 31°C			m d^{-1}
		carbon/nitrogen detritus	20.0	
		silica detritus	50.0	
		iron detritus	20.0	
r	Remineralization rate at 20°C			d^{-1}
		carbon/nitrate	0.02	
		silica	0.0001	
		iron	0.02	
Φ	Carbon:chlorophyll ratio		Variable	g g^{-1}

NASA Ocean Biogeochemical Model (NOBM)
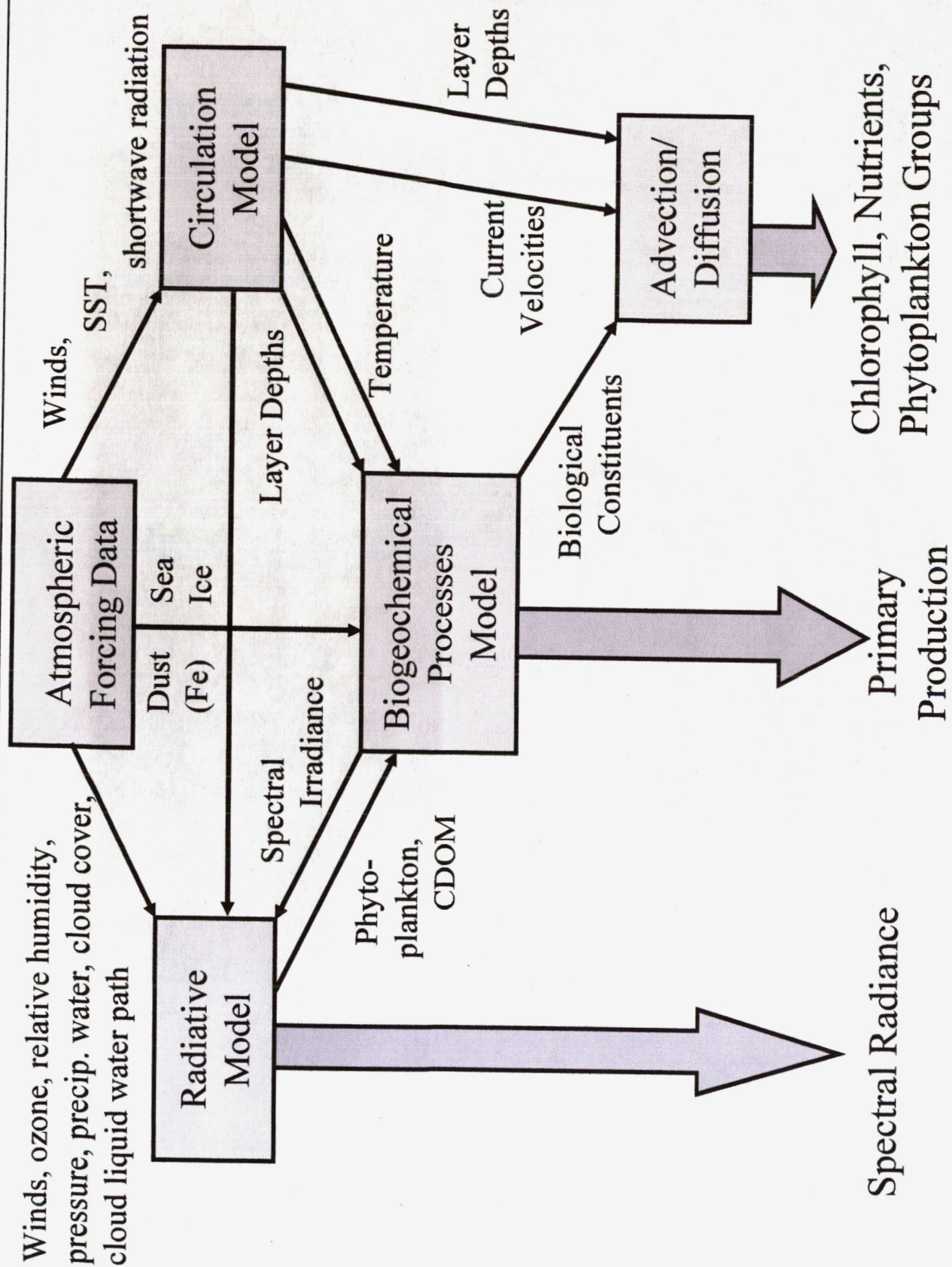
Figure 1. Pathways and interactions among the components of the NASA Ocean Biogeochemical Model (NOBM).

Biogeochemical Processes Model
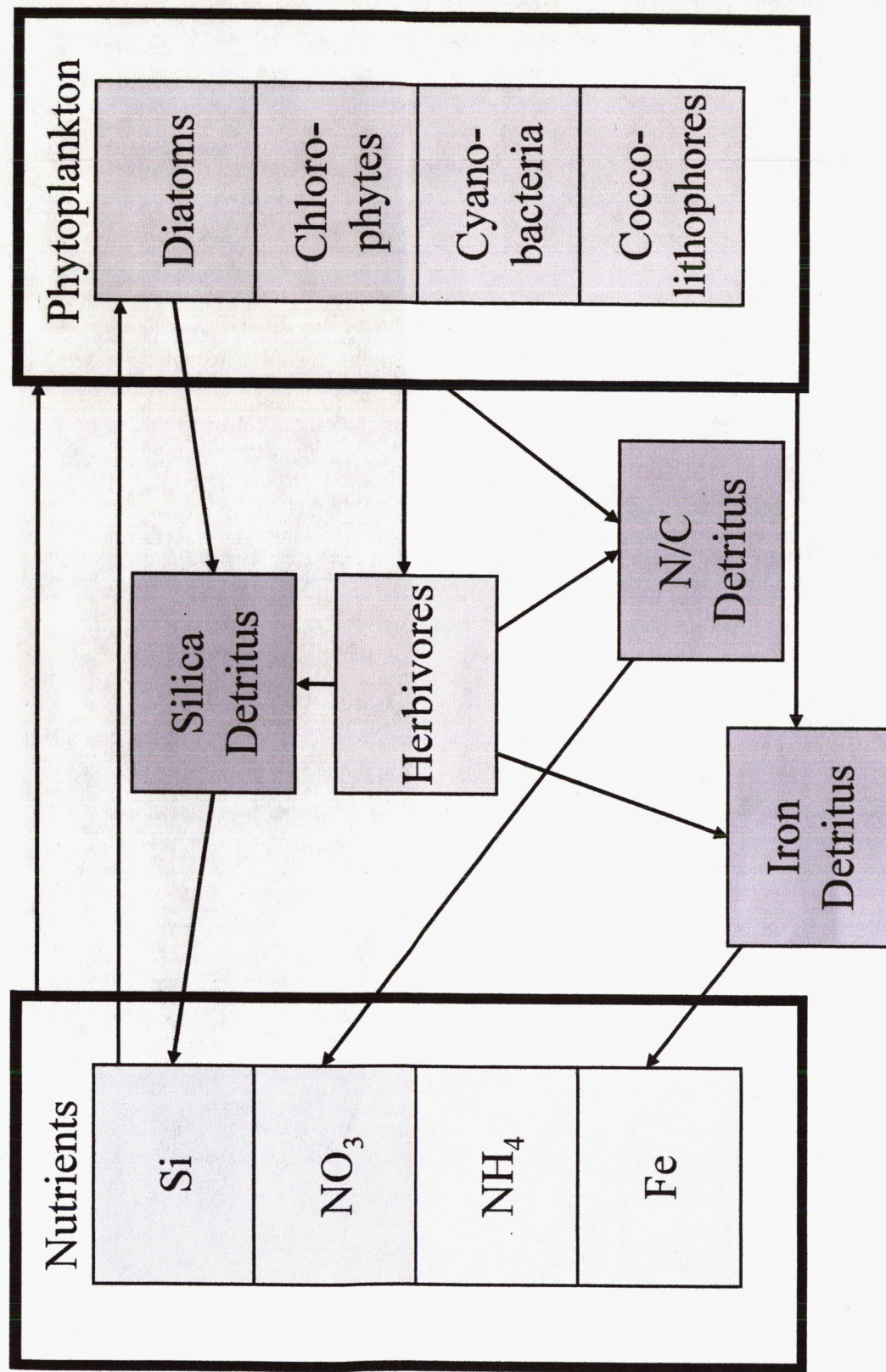
Figure 2. Pathways and interactions among the components of the Biogeochemical Processes model, comprising 4 phytoplankton groups, 4 nutrient groups, a single herbivore group and 3 detrital components.

Model Weighting Factors January
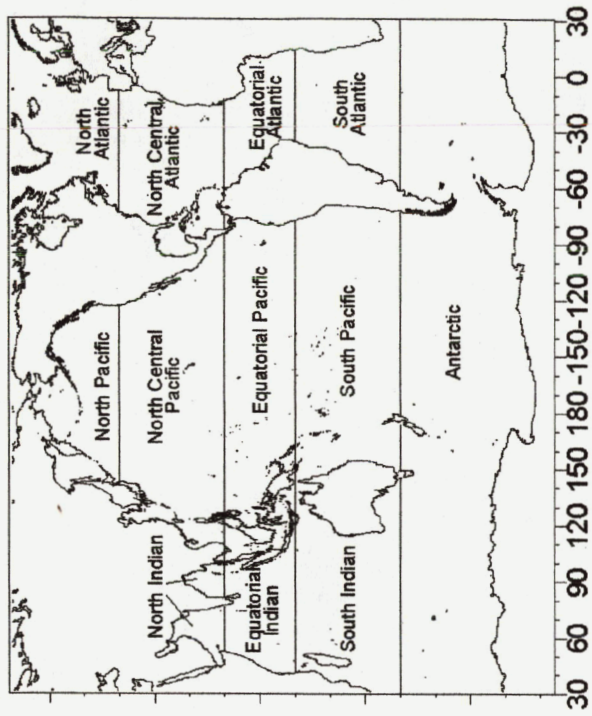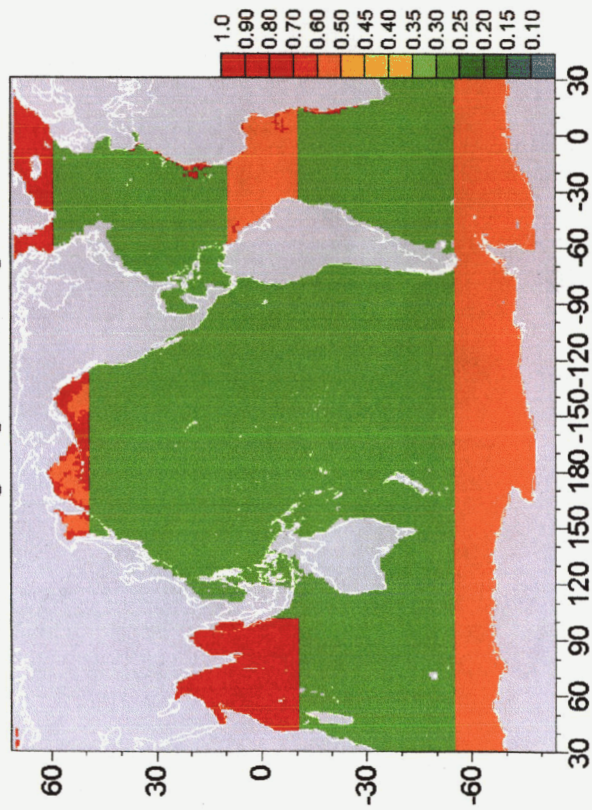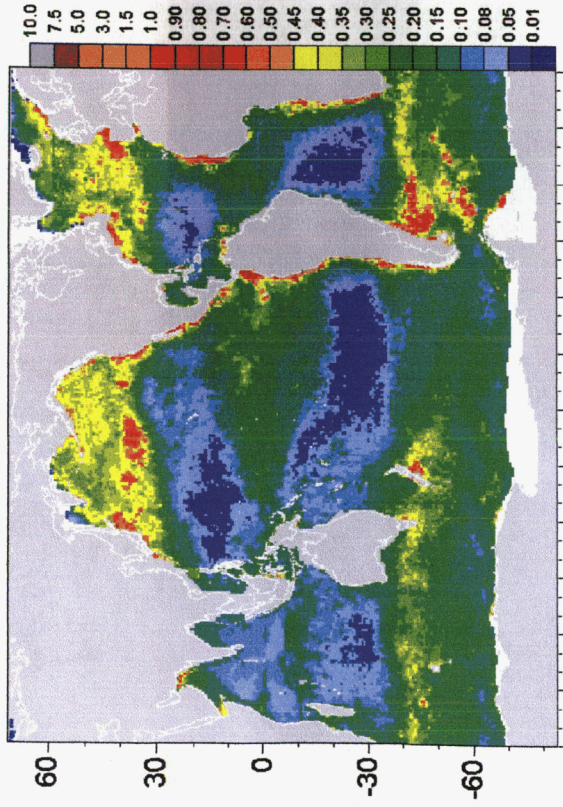
Model Weighting Factors June

Model Weighting Factors August

North Pacific
North Central Pacific
Equatorial Pacific
South Pacific
Antarctic

North Atlantic
North Central Atlantic
Equatorial Atlantic
South Atlantic

North Indian
Equatorial Indian
South Indian

Figure 3. Regional model weighting factors along with delineation of the major oceanographic basins.

Free Run Model Chlorophyll Apr 1 200

Assimilated Chlorophyll Apr 1 2001

Daily SeaWiFS Chlorophyll Apr 1 2001
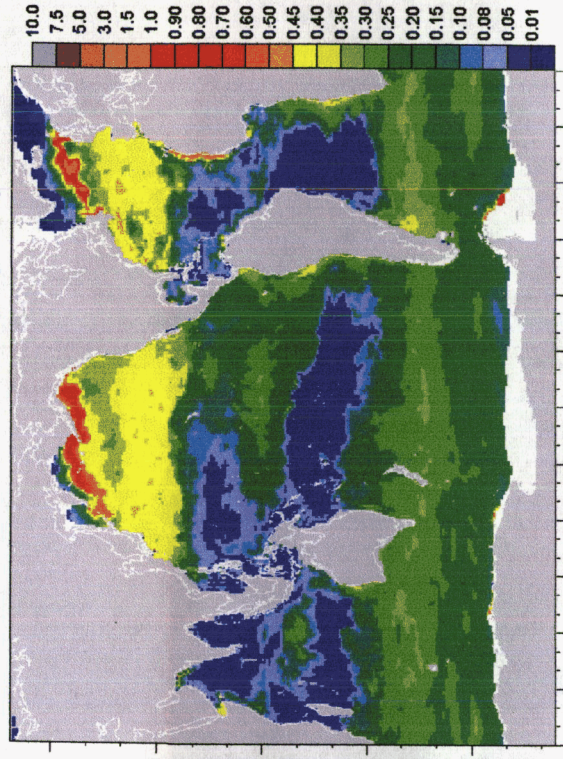
Monthly SeaWiFS Chlorophyll Apr 2001
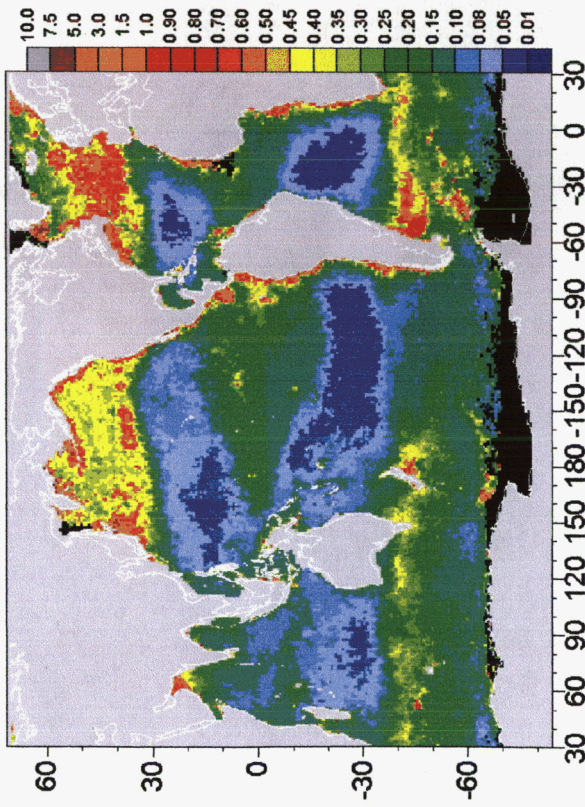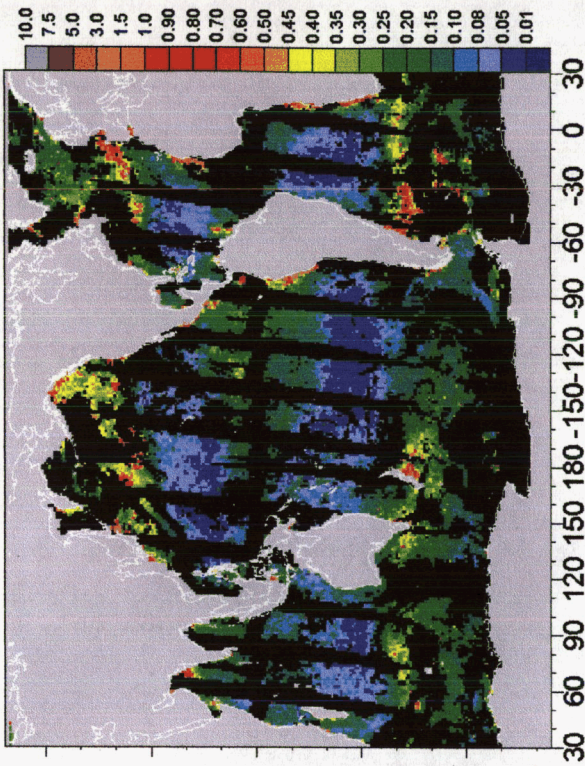
Figure 4. Comparison of chlorophyll (mg m⁻³) from the assimilation model, the free-run model, and SeaWiFS. The assimilation and free-run chlorophyll distributions represent simulations for April 1, 2001. SeaWiFS data for the same day are shown for comparison, along with the monthly mean. Grey indicates land and coast, black indicates missing data, and white indicates sea ice.

SeaWiFS Chlorophyll Mar 2001

7.5	
5.0	
3.0	
1.5	
1.0	
0.90	
0.80	
0.70	
0.60	
0.50	
0.45	
0.40	
0.35	
0.30	
0.25	
0.20	
0.15	
0.10	
0.08	
0.05	
0.01	

Assimilated Chlorophyll Mar 2001
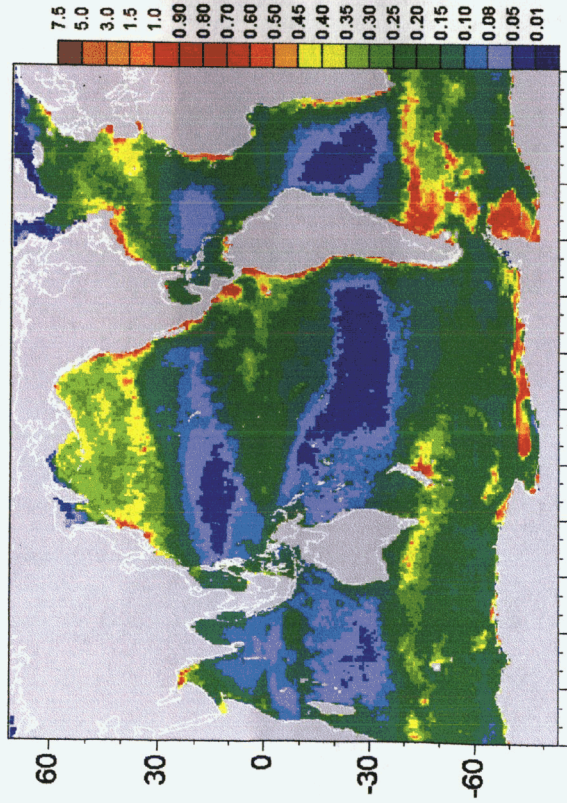
7.5	
5.0	
3.0	
1.5	
1.0	
0.90	
0.80	
0.70	
0.60	
0.50	
0.45	
0.40	
0.35	
0.30	
0.25	
0.20	
0.15	
0.10	
0.08	
0.05	
0.01	

Difference (Assim-SeaWiFS) Mar 2001

10.0	
5.0	
1.0	
0.75	
0.50	
0.40	
0.30	
0.20	
0.10	
0.05	
0.01	
-.01	
-.05	
-.10	
-.20	
-.30	
-.40	
-.50	
-.75	
-1.0	
-5.0	

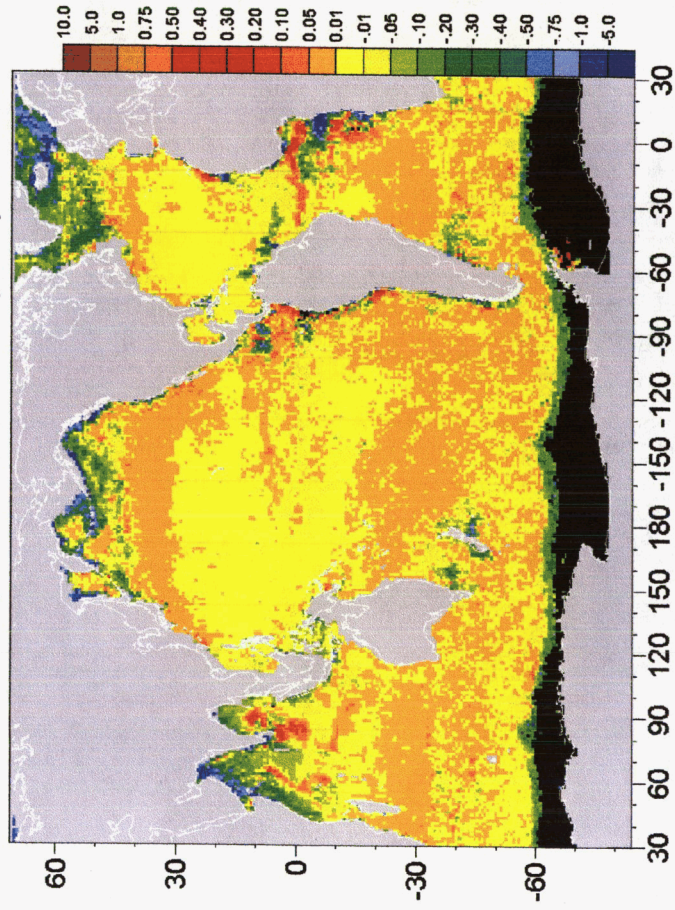Fig. 5. Assimilation model chlorophyll (mg m^{-3}), SeaWiFS mean chlorophyll, and the difference (Assimilation-SeaWiFS) for March 2001

Fig. 6. Assimilation model chlorophyll (mg m⁻³), SeaWiFS mean chlorophyll, and the difference (Assimilation-SeaWiFS) for Sep 2001.
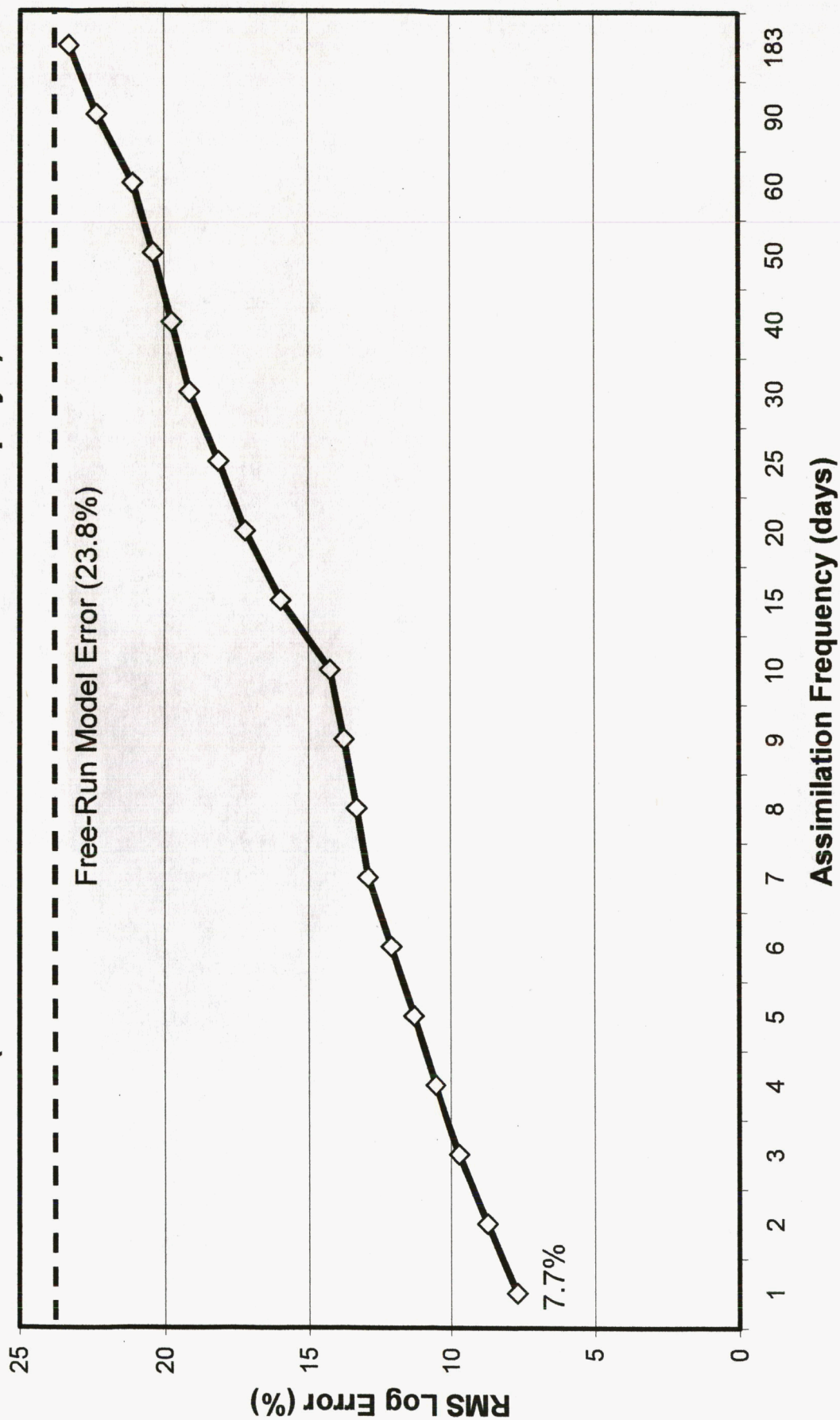
Figure 7. Annual RMS log error for assimilation as a function of assimilation frequency (number of days when assimilation is performed). The annual RMS log error for the free-run model is shown.
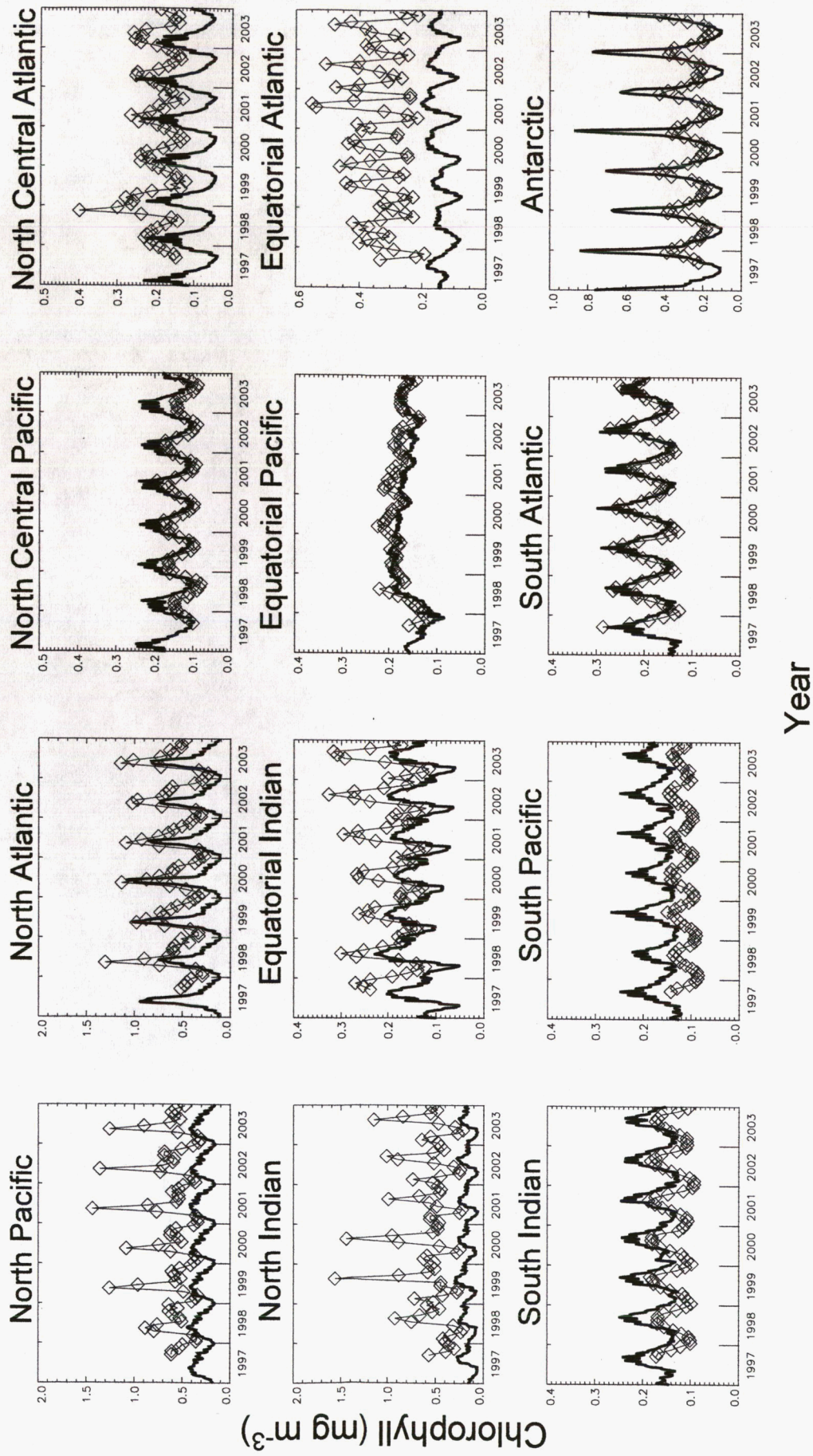
Figure 8. a) SeaWiFS monthly mean chlorophyll (diamonds) and daily chlorophyll from the free-run model (solid line) for 1997-2003.
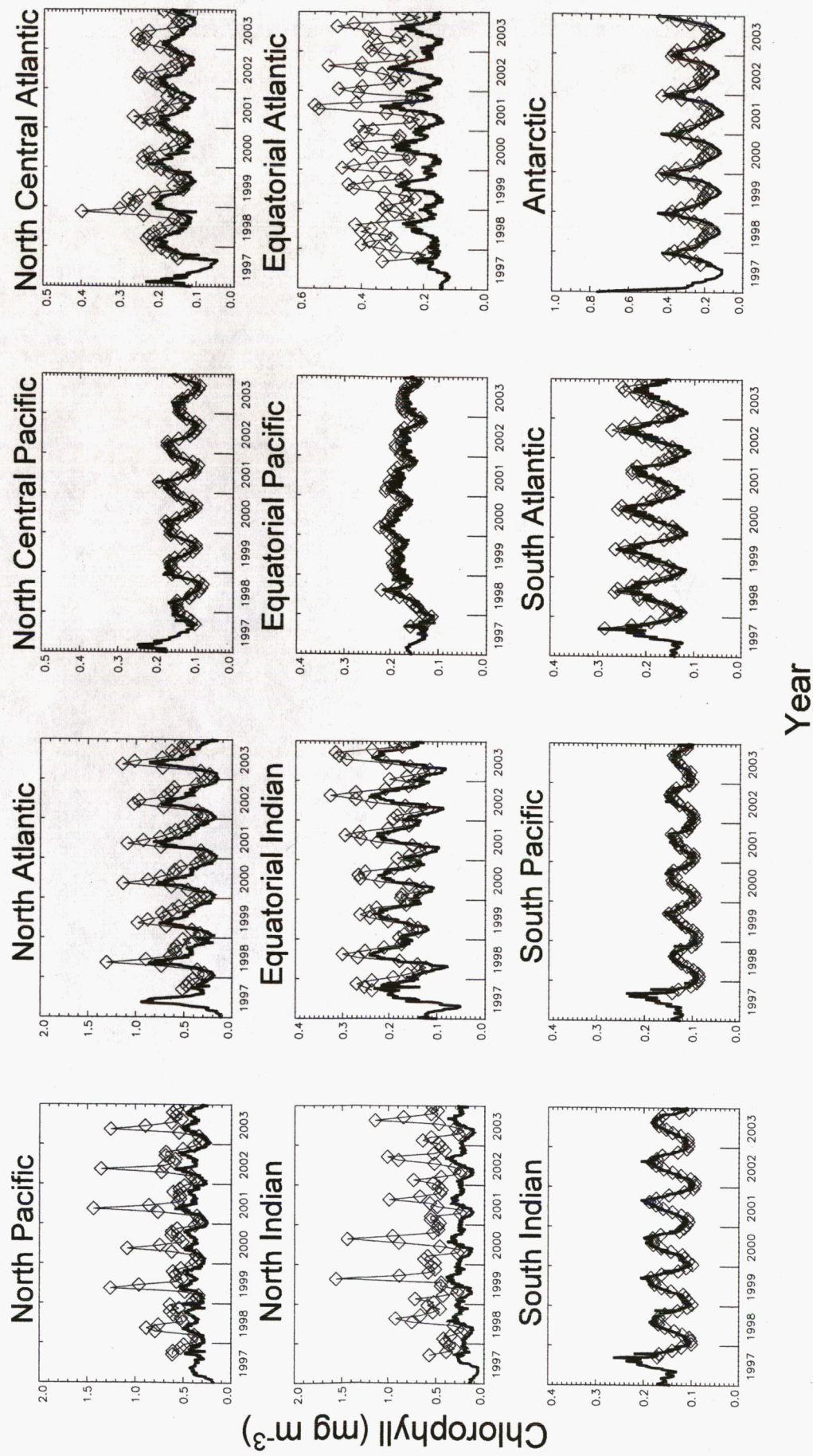
Figure 8. b) SeaWiFS monthly mean chlorophyll (diamonds) and daily chlorophyll from the assimilation model (solid line) for 1997-2003. Assimilation of SeaWiFS chlorophyll did not begin until September 1997 (beginning of SeaWiFS data collection).
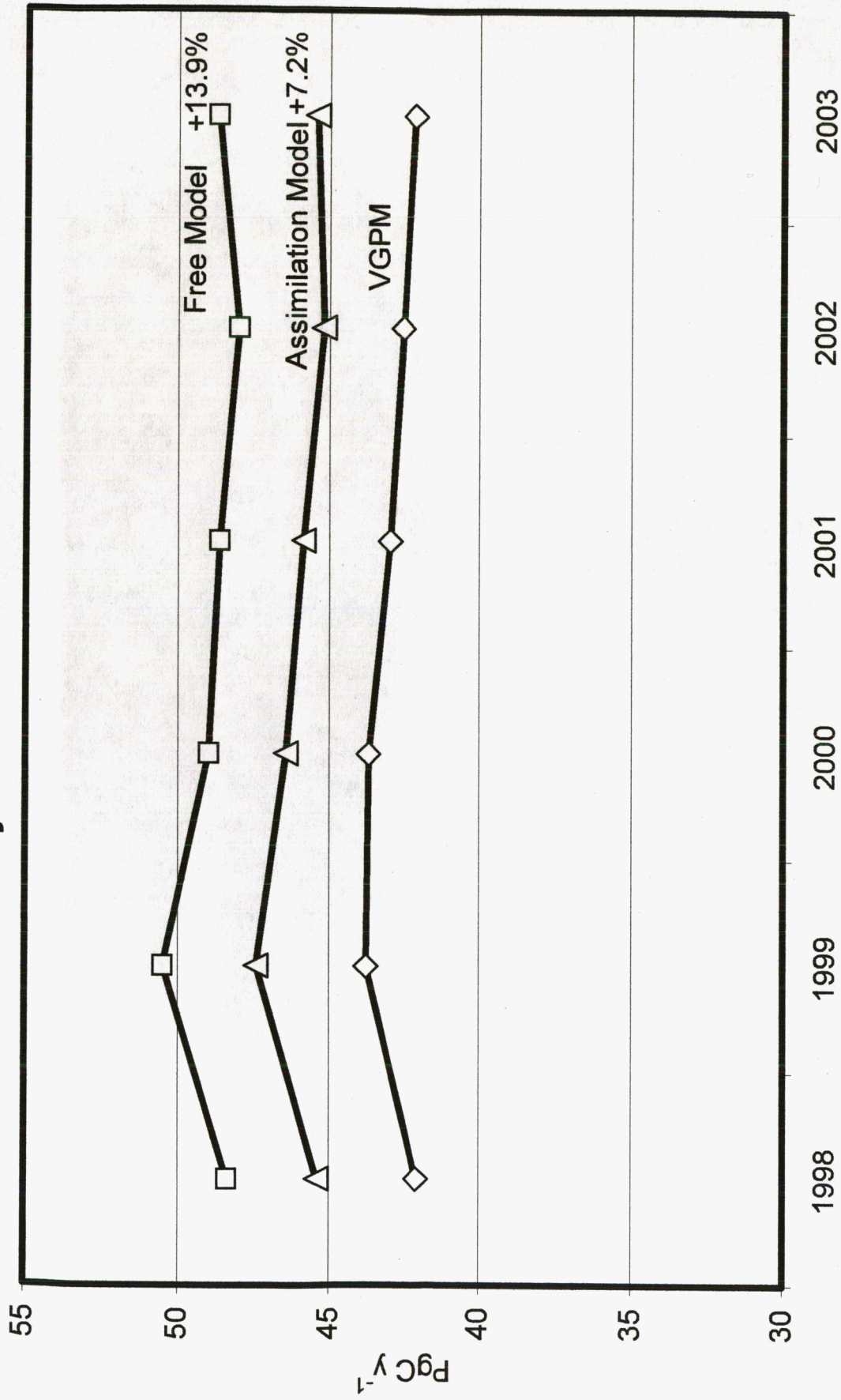
Figure 9. Annual primary production for the period 1998-2003 from the VGPM, free-run model, and assimilation model. The mean departures over the period for the free-run model and assimilation model are indicated.